Total and partial pion absorption cross sections on ^{4}He in the Δ resonance region

A. O. Mateos,[5] D. Androić,[9] G. Backenstoss,[1] D. Bosnar,[9] H. Breuer,[4] H. Döbbeling,[8] T. Dooling,[7] M. Furić,[9] P. A. M. Gram,[3] N. K. Gregory,[5] A. Hoffart,[2,8] Q. Ingram,[8] A. Klein,[7] K. Koch,[8] J. Köhler,[1] B. Kotliński,[8] M. Kroedel,[1] G. Kyle,[6] A. Lehmann,[1,8] K. Michaelian,[8] T. Petković,[9] M. Planinić,[9] R. P. Redwine,[5] D. Rowntree,[5] U. Sennhauser,[8] N. Simičević,[5] R. Trezeciak,[2] H. Ullrich,[2] M. Wang,[6] M. H. Wang,[6] H. J. Weyer,[1] M. Wildi,[1] and K. E. Wilson[5]

(LADS Collaboration)

[1]*University of Basel, CH-4056 Basel, Switzerland*
[2]*University of Karlsruhe, D-76128 Karlsruhe, Germany*
[3]*LAMPF, Los Alamos, New Mexico 87545*
[4]*University of Maryland, College Park, Maryland 20742*
[5]*Massachusetts Institute of Technology, Cambridge, Massachusetts 02139*
[6]*New Mexico State University, Las Cruces, New Mexico 88003*
[7]*Old Dominion University, Norfolk, Virginia 23529*
[8]*Paul Scherrer Institute, CH-5232 Villigen PSI, Switzerland*
[9]*University of Zagreb, HR-10000 Zagreb, Croatia*

(Received 2 September 1997)

This paper presents a large solid angle measurement of the positive pion absorption cross section on ^{4}He and its decomposition into partial channels. The total absorption cross sections at incident pion kinetic energies of $T_{\pi^+}=70$, 118, 162, and 239 MeV are 35 ± 5, 52 ± 4, 51 ± 5, and 27 ± 2 mb, respectively. These values are lower than those reported in some previous experiments. At all pion energies a large fraction of the absorption cross section is due to multinucleon channels. [S0556-2813(98)03108-2]

PACS number(s): 25.80.Ls, 14.20.Gk

I. INTRODUCTION

Because of energy and momentum conservation, pion absorption is kinematically forbidden on a free nucleon and is highly suppressed on a single nucleon in the nucleus. Thus, in lowest order, pion absorption must take place on at least two nucleons. Several experiments in the 1980's have shown, however, that a significant fraction of the absorption cross section consists of events in which three or more nucleons carry away a substantial amount of the energy [1,2].

The study of pion absorption on few-body systems provides the most direct means of elucidating the reaction mechanisms involved in multinucleon pion absorption. The study of pion absorption on ^{3}He allows one to examine the contribution from three-nucleon absorption (3NA), in which all three of the final state nucleons share the momentum and energy of the incoming pion in a substantial way. Several small solid angle, kinematically complete measurements on ^{3}He in the $\Delta(1232)$ resonance region have reported that the energy distribution of about one-quarter of the absorption cross section appears consistent with three-nucleon phase space [3–8]. Recent large solid angle measurements of the pion absorption cross section on ^{3}He [9–12] have shown that there is a significant, but not dominant, contribution to the 3NA cross section from a process in which the pion initially interacts with one of the nucleons [initial state interaction (ISI)] before being absorbed on a deuteronlike pair. The contribution from events in which there is a nucleon-nucleon final state interaction (FSI) after the absorption of the pion does not appear to be strong, and thus a large fraction of the 3NA cross section remains unexplained.

Although the experimental facts surrounding π^+ absorption on ^{3}He in the resonance region are now fairly well established, the reaction on that nucleus is restricted to the one final state with three protons. Thus, for the investigation of the nature of multinucleon absorption, the reaction on ^{4}He is more representative of the situation in heavier nuclei, while still being reasonably simple. Specifically, in ^{4}He absorption on $T=1$ nucleon pairs is possible in 2NA and the $T=1/2$ final state is accessible in 3NA; in addition the four-nucleon absorption reaction (4NA) is possible, a channel which has been suggested could be strong [13,14]. Furthermore, the much increased nuclear density might also enhance dynamics not favored in ^{3}He. Finally, ^{4}He may be the heaviest nucleus where it is possible to completely define experimentally the kinematics of most of the final states. Understanding pion absorption processes in ^{4}He is, however, more complicated compared to the case of ^{3}He partly because of the possibility of deuteronic final states.

The absorption reaction on ^{4}He is less well understood than that on ^{3}He, and even the data on the total absorption cross section do not agree well [15–19]. A study of the contributions of partial absorption cross sections to the total has been reported by one small solid angle experiment at 118 MeV [19], using large extrapolations of the measured distributions, while other experiments [20–24] have provided some partial cross sections at several energies. In this paper we report a measurement of the total π^+ absorption cross section on ^{4}He and its decomposition into channels according to the number of participating nucleons and the final state, for incident positive pion kinetic energies of 70, 118, 162, and 239 MeV.

II. EXPERIMENT

The experiment was carried out at the πM1 channel at the Paul Scherrer Institute (PSI), using the Large Acceptance

Detector System (LADS). This detector was designed to study multiparticle states following pion absorption, and its large solid angle and low energy threshold allowed the determination of the integrated cross sections with only small extrapolations of the measured distributions. For the case of ^{4}He, it was possible to completely reconstruct the kinematics of the final state for most absorption reaction channels.

As it is described in detail elsewhere [25], only general aspects of the detector are summarized here. The LADS detector was cylindrical in shape with an active volume 1.6 m long. It consisted of 28 $\Delta E-E-E$ plastic scintillator telescopes packed closely together to form a cylinder. Photomultipliers were mounted on both ends of the scintillators allowing the determination of the time-of-flight for detected particles. To increase the total solid angle coverage, annular endcap detectors with entrance and exit holes for the beam were inserted at each end of the cylinder. The solid angle coverage of the detector was 98% of 4π. Two coaxial cylindrical wire chambers provided tracking information for charged particles with an angular resolution of about $1°$ and a vertex resolution of 1 mm. The energy threshold for detected charged particles was roughly 20 MeV and the energy resolution for charged particles was 3–5 % full width at half maximum (FWHM). Neutrons, detected with a probability of roughly 35% for energies above 12 MeV, were distinguished from photons by time-of-flight. Neutron azimuthal and polar angles were determined within $\pm 7°$. The target used in the experiment consisted of a 4 cm diameter, 25.7 cm long carbon fiber cell with walls of 0.5 mm thickness, containing ^{4}He at a pressure of 100 bar.

The incident beam was defined using plastic scintillator detectors which counted individual pions; these were identified by time-of-flight and pulse-height analysis. A 2 cm diameter counter 50 cm upstream of the target center defined the size of the beam, and sets of counters upstream of LADS ensured that only single incident particles were counted as valid beam pions. From a total incident flux of about 3×10^6/sec, the defined beam rate was typically 1×10^5/sec. Events were classified in the trigger logic according to the number of charged and neutral particles detected in LADS in coincidence with a valid incident pion. The various event types were then prescaled individually according to the physics interest of the information they contained.

III. EXTRACTION AND NORMALIZATION OF THE DATA

A. Extraction of absorption events

To determine the absorption cross sections, the events originating from the target gas were first selected and those from nonabsorption reactions removed. The reconstructed interaction vertex position was used to eliminate events from the target end walls, while data from empty target runs were used to subtract those from the cylindrical target walls. The magnitude of the empty target subtraction varied with the beam energy and the numbers of particles detected, but was typically less than 5%. Events containing charged pions were removed from the sample by time-of-flight and dE/dx vs E particle identification techniques, reducing the charged pion contamination to typically less than 2%. After the application of cuts on the missing mass, missing momentum, and missing energy, contamination by events containing neutral or charged pions was reduced to an insignificant level. More detailed information on the procedure used for the extraction of pion absorption events can be found in Refs. [26–29].

B. Normalization

Once the absorption events were isolated, the measured raw counts were normalized to the number of incident pions and target scatterers to yield a raw cross section. The number of incident pions was counted by the beam defining counter. Corrections were made to account for contamination in the beam, for the number of pions lost through decay or reactions before reaching the target, and for pions missing the target. The largest systematic uncertainty in the determination of the beam normalization resulted from this last correction. It was measured by examining the radial distribution of events from the air upstream and downstream of the target, and the uncertainty in this correction ranged between 3 and 12 %. The number of target scatterers was determined from measurements of the pressure and temperature of the target. The areal density of the target was typically 4.5×10^{22} nuclei/cm^2, and was known with an uncertainty of 1%. In addition, various combinations of charged and neutral particles in the detector were prescaled in the trigger to enhance events of physics interest over background. A correction for this was applied for each trigger type to yield the raw cross section [26–29]. The reliability of the extraction and normalization procedures was verified by a measurement of the well known pion absorption cross section on deuterium.

IV. ANALYSIS

The goal of the analysis discussed here was to provide total and partial absorption cross sections, the latter classified according to which particles participated in the reaction. Participating particles were usually emitted with high momenta, while spectators had momentum distributions consistent with those found in the ground state of the ^{4}He nucleus. Since the final state momentum distributions of the partial cross section classes overlapped each other kinematically, the decomposition of the final states into these classes was done with the help of reaction models. The final state distributions generated from these models were fit to the data, and the partial cross sections for the entire kinematic region were determined. The reaction models used will be described in Sec. IV C. Before describing the data analysis it is useful to clarify the meaning of terms that will be used.

A. Classification and nomenclature

For the π^+-^{4}He absorption reaction there are three possible final states: $ppppn$, ppd, and p^3He. The cross section for absorption leading to the p^3He final state is small (see, e.g., Ref. [19]) and will not be considered further here. Components of the two other final states are then distinguished here according to the following.

(i) The ''physics channel,'' a classification of a final state according to the particles which have participated in the absorption reaction, which are the partial cross sections given in this paper. Physics channels are denoted in this paper using parentheses. Thus an event in which particles a and b

participated, while particle c was only a spectator, belongs to the $(ab)c$ physics channel. The physics channels considered in this analysis are $(pp)pn$, $(pp)d$, $(pn)pp$, $(ppp)n$, $(ppn)p$, $(pppn)$, $(pd)p$, and (ppd).

(ii) The ''detected channel,'' a classification according to the number of particles detected in the experiment. These are denoted in boldface. An event in which only three protons were detected would be classified as being in the **(ppp)n** detected channel. Because of the low energy threshold and large solid angular acceptance of the LADS detector there is a strong correspondence between the detected channels and the number of participating and spectating particles. Participants tend to be above the detector threshold and spectator particles tend to be below it. For example, the **(ppp)n** detected channel is largely populated by the $(ppp)n$ physics channel, with some contribution from $(pp)pn$, $(ppn)p$, and $(pppn)$.

(iii) The ''selected channel,'' a subset of one or more detected channels, in which certain kinematic conditions have been imposed to enhance the importance of one or more physics channels in the selected data. Selected channels are denoted by square brackets. Thus the selected channel $[ppp]$ consists of those parts of the detected channels **(ppp)n** and **(ppp)n** where all the protons have more than 30 MeV and the neutron momentum is less than 250 MeV/c. The imposed kinematic cuts selectively enhance the fractional contribution from $(ppp)n$ so that it dominates the selected channel. The specific definition of each of the selected channels is given in Sec. IV B.

B. Selected channels

As mentioned above, for the determination of the cross section of the physics channels, selected channels were defined which enhanced the fraction of one or two physics channels. This resulted in kinematic distributions dominated by these one or two physics channels, which was particularly useful in the comparison with models used in the analysis to simulate these channels. The selected channels used in the analysis are summarized below.

Selected $[pp]$. This contained events from the detected **(pp)pn/d** channels, where the missing momentum was less than 250 MeV/c and a cut was placed requiring the sum of the two proton energies to be roughly 50 MeV above the incident pion kinetic energy. In addition, the opening angle between the two protons was required to be greater than 140° in their center of mass system.

Selected $[ppp]$. This contained events from the detected **(ppp)n** and **(pppn)** channels, with each proton having at least 30 MeV kinetic energy, and the invariant missing mass, always calculated from the momenta of the three protons, being equal to the neutron mass. The momentum of the neutron was also always reconstructed from the momenta of the three protons, and was required to be less than 250 MeV/c.

Selected $[ppn]$. This contained events from the detected **(ppn)p** channel, with each detected proton having at least 30 MeV kinetic energy. The magnitude of the neutron momentum and the momentum vector of the undetected proton were reconstructed from the momenta of the detected protons and the direction of the neutron. The reconstructed neutron energy was required to be greater than 30 MeV and the momentum of the undetected proton less than 250 MeV/c.

Selected $[pppn]$. This contained events satisfying the same requirements as those in the $[ppp]$ channel, except that the reconstructed neutron momentum was above 250 MeV/c.

Selected $[ppd]$. This contained events from the detected **(ppd)** channel, with a cut requiring the sum of the kinetic energies to be roughly 50 MeV larger than the kinetic energy of the incident pion.

Selected $[pd]$. This contained events from the detected **(pd)p** channel, with a cut requiring the sum of the measured kinetic energies to be roughly 35 MeV above the incident pion kinetic energy, and with the missing momentum of the undetected proton required to be under 200 MeV/c. The missing momentum cut was chosen to be 50 MeV/c lower than that used to define spectators in other selected channels to eliminate contamination in the data attributable to π-d knockout from ^{4}He in which the deuteron is detected and the pion absorbed in the scintillator.

The raw cross sections for each of the selected channels at each measured energy are shown in Table I. The differences between the raw cross sections given here and the final results given in Table II (Sec. V) indicate the combined size of the corrections to the data for inefficiencies and extrapolations due to missing solid angle and particles being below threshold.

TABLE I. The raw cross sections (in mb) in the six selected channels. These are the cross sections before any acceptance corrections or decompositions into physics channels are performed.

Selected channel	70 MeV	118 MeV	162 MeV	239 MeV
$[pp]$	14.6	18.7	16.5	5.3
$[ppp]$	0.6	1.3	2.3	1.7
$[ppn]$	0.6	1.2	1.8	1.0
$[pppn]$	0.1	0.4	0.8	0.9
$[pd]$	1.5	1.3	0.8	0.1
$[ppd]$	1.2	2.1	2.1	0.8
Total	18.7	24.9	24.3	10.0

C. Simulations and fits to the data

To obtain the partial and total absorption cross sections from the raw cross sections, Monte Carlo simulations of the

TABLE II. Decomposition of the total absorption cross section, according to the reaction participants. The results for $(ppp)n$, $(ppn)p$, and $(pppn)$ are taken from Ref. [39]. All cross sections are in mb.

Physics channel	70 MeV	118 MeV	162 MeV	239 MeV
$(pp)d/pn$	19.9±3.2	28.4±2.6	24.1±2.5	10.9±1.0
$(ppp)n$	2.0±0.7	3.8±0.5	5.9±0.7	4.3±0.4
$(ppn)p$	7.2±1.3	9.8±1.3	10.9±1.4	6.0±0.7
$(pppn)$	0.6±0.3	1.7±0.2	1.7±0.5	2.2±0.2
$(pd)p$	2.5±0.4	2.5±0.2	2.1±0.2	0.8±0.1
(ppd)	2.2±0.3	4.1±0.3	4.2±0.4	1.5±0.1
$(pn)pp$	0.6±0.3	1.8±0.9	1.6±0.8	0.9±0.4
Total	35±5	52±4	51±5	27±2

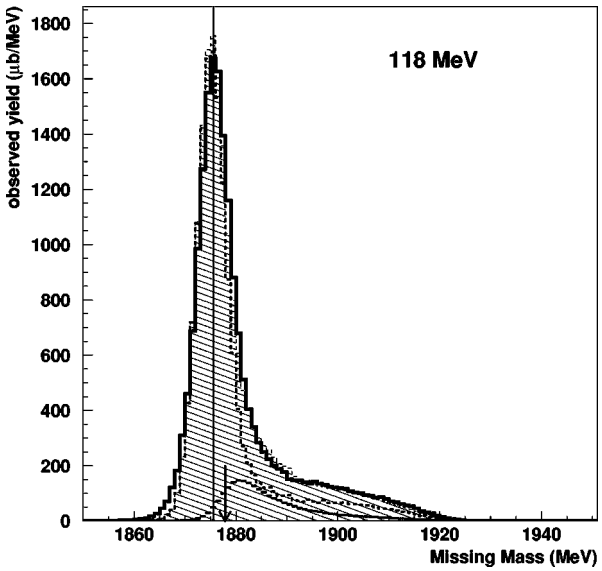

FIG. 1. The missing mass reconstructed from two observed protons in the selected $[pp]$ channel. The dark solid line is the data, the hatched distribution is the sum of the fitted Monte Carlo distributions. The dashed line is the contribution from $(pp)d$ and the light solid line the contribution from $(pp)pn$. The vertical line indicates the deuteron mass and the arrow the pn end point. The yield has not been corrected for detector acceptance and losses, nor for the effects of the kinematic cuts applied.

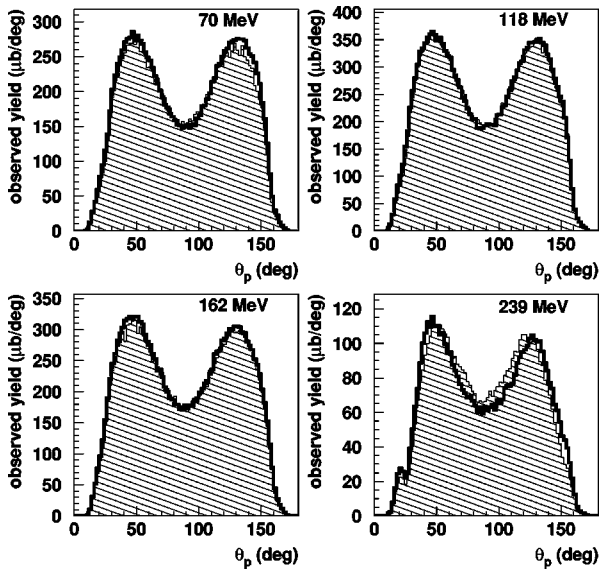

FIG. 2. The polar angle θ of the two protons from the selected $[pp]$ channel in the π-d center-of-mass system. The dark solid line is the data, the hatched histogram the sum of the fitted Monte Carlo distributions. The yields have not been corrected for detector acceptance and losses, nor for the effects of the kinematic cuts applied.

data were performed. The inputs to these simulations were models of various absorption processes, together with a description of the detector including all inefficiencies, thresholds, and geometrical acceptances [26,28]. The partial cross sections were determined by fits of the modeled absorption processes to the data. The relative contributions of these modeled processes to the detected cross sections, folded with corrections for detector efficiency and acceptance limitations, yielded the partial cross sections.

In this analysis only a few absorption processes were modeled, providing reasonable descriptions of the data. The $(pp)d$ and $(pp)pn$ channels were modeled as 2NA with absorption occurring on a quasideuteron inside the ^{4}He nucleus, using Ritchie's parametrization [30] of absorption on a deuteron, with either a spectator d or spectator pn pair (using single nucleon and deuteron momentum distributions calculated by Schiavilla [31]). For the other channels the simplest models consistent with the data were used, since the corrections for inefficiencies and acceptances were generally not strongly sensitive to the model assumption. This insensitivity was also the case for the separation of events into the different physics channels (i.e., the partial cross sections given here).

The four-body final state channels $(ppp)n$, $(ppn)p$, and $(pppn)$ were modeled using four-nucleon phase space distributions, with additional weights for the first two such that the spectators had the single particle momentum distribution of ^{4}He. These were additionally weighted with the Jost enhancement functions F_{pp} and F_{pn} [32–34] to account for the effects of soft final state interactions [35–37] with standard parametrizations of the effective range and scattering length [38], as described in Ref. [12]. The agreement between the energy distributions obtained from the data and the simple models was in general good. Some deviations were, however, seen between the simple phase space distributions and the observed angular distributions. Because of the large solid angle covered by the experiment, extrapolations due to missing solid angle were small.

For the multinucleon channels involving a deuteron in the final state, the generators were empirically modified to give distributions matching those observed experimentally. The $(pd)p$ channel was modeled as 2NA followed by neutron pickup by an exiting proton, with the remaining proton as a spectator. In the data, deuterons appeared preferentially backward and so an additional weighting of the simulation by their angular distributions was required in order to obtain a reasonable description. Similarly, the (ppd) three-body phase space distributions were modified by an additional weight to take into account the peaking of the deuteron energy toward lower energies which was observed in the data.

After generation according to the various models, the particles were tracked through a simulation of the detector which included realistic resolutions and the digitization of outputs of various detector components. The simulated data were then run through the same analysis program used to analyze the experimental data, and identical cuts were applied to both. The simulations and the experimental data were thus subject to the same thresholds, geometrical acceptance effects, reaction losses, efficiencies for particle detection and identification, and wire chamber and software reconstruction inefficiencies [26,28]. The uncertainty on the cross section determination associated with using the Monte Carlo simulation for these corrections was assessed by comparison with selected data samples in which the kinematics was overdetermined. This uncertainty was estimated to be about 6%.

The relative strengths of the seven different physics processes were determined by simultaneous fits to kinematic distributions from the six selected channels, with the normal-

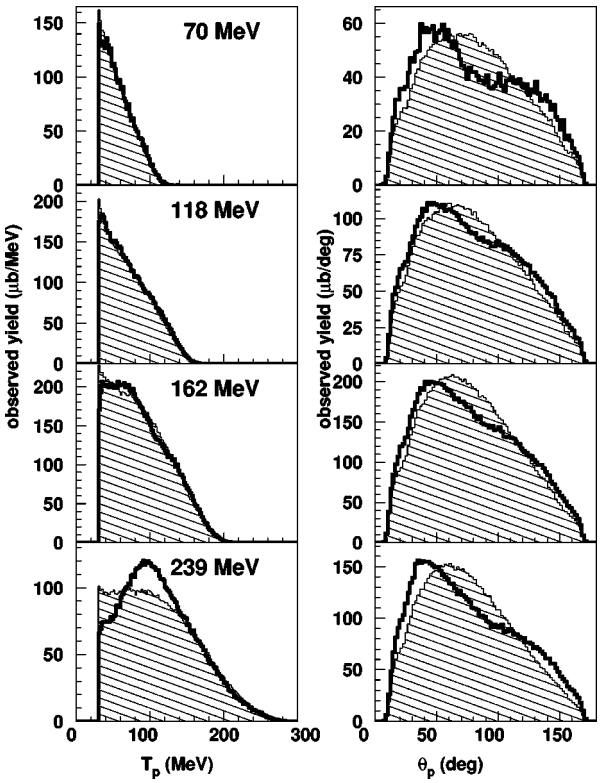

FIG. 3. The laboratory kinetic energy and θ distributions of the three protons for the selected $[ppp]$ channel, as in Fig. 2.

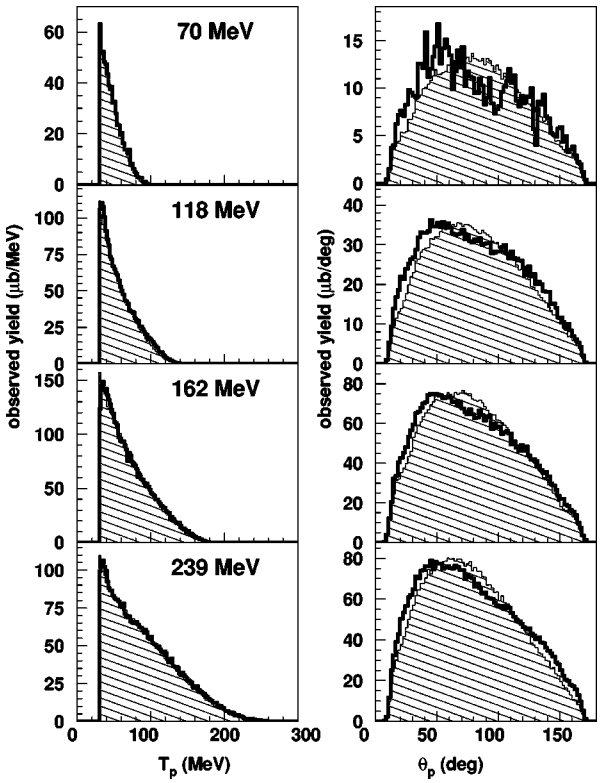

FIG. 4. The laboratory kinetic energy and θ distributions of the three protons for the selected $[pppn]$ channel, as in Fig. 2.

izations of the seven processes as free parameters. The simultaneous fit was performed over three different histogram sets for the selected channels, including both one and two-dimensional histograms. The histograms in the various sets included among other things the sum of the energies of the detected particles, the missing momenta, the energy and angle distributions of the particles, opening angles, and energy-angle correlations.

The analysis was repeated on the three histogram sets with three different thresholds defining the selected channels. Kinetic energy thresholds, missing mass, and total energy cuts were raised and lowered by 10 MeV and missing momentum thresholds were varied by ± 50 MeV/c from the central values defining the selected channels as given in Sec. IV B. The average value obtained from the simultaneous fits with different histogram sets and thresholds was taken as the result for the contribution from each physics channel. The uncertainty associated with the fitting procedure was estimated from the variation of the results obtained under the different conditions. For a given quantity, it was taken to be the standard deviation of the results obtained from the nine simultaneous fits. Figures 1 –10 show one-dimensional kinematic distributions for the selected channels as an indication of the quality of the fits to the data.

D. Estimate of $(pn)pp$ absorption

The relatively weak $(pn)pp$ absorption channel was not well measured; because of large background at the trigger level, candidate events were strongly suppressed by prescaling. For this reason, the $(pn)pp$ channel was not included in the global fit procedure and we were only able to make rough estimates of its contribution.

Events were selected in which there was a proton with a kinetic energy of at least 100 MeV, a neutron, and no photon. Using the momentum and angle information of the proton and the angle information from the neutron, the momen-

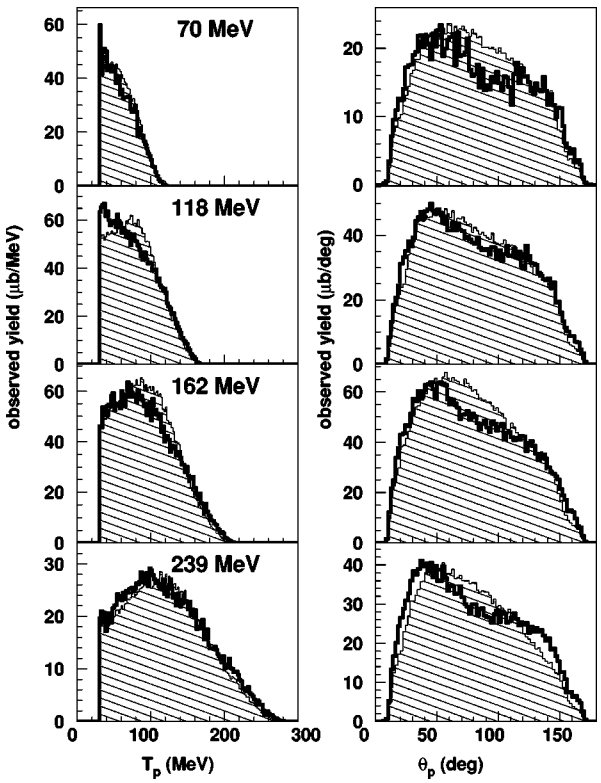

FIG. 5. The laboratory kinetic energy and θ distributions of the two protons from the selected $[ppn]$ channel, as in Fig. 2.

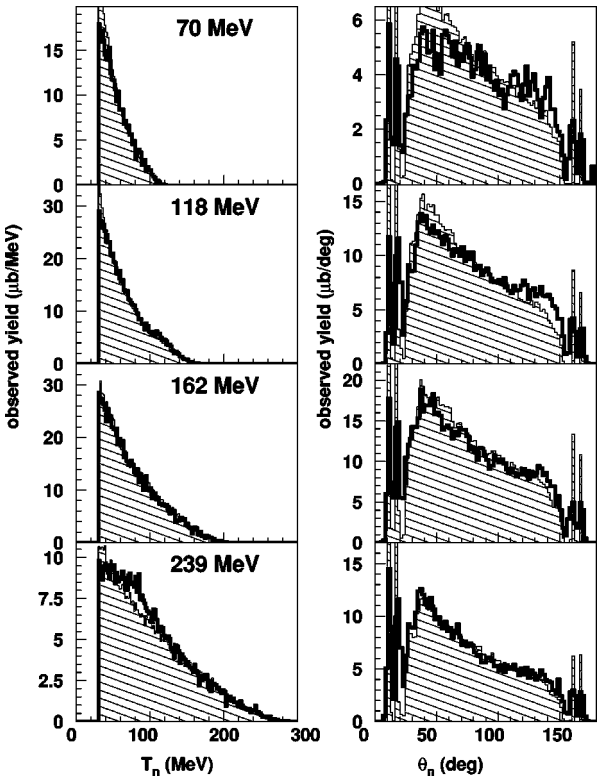

FIG. 6. The laboratory kinetic energy and θ distributions of the neutron from the selected $[ppn]$ channel, as in Fig. 2.

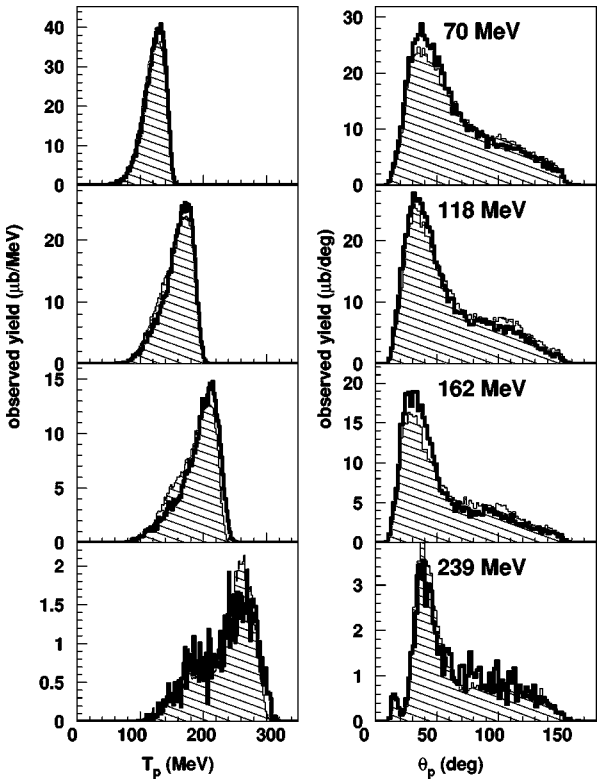

FIG. 8. The laboratory kinetic energy and θ distribution of the proton in the selected $[pd]$ channel, as in Fig. 2.

tum of the neutron and the momentum of the unobserved unbound pp system were reconstructed. The missing momentum of the unobserved pp pair was required to be below 300 MeV/c to obtain the selected $[pn]$ channel. Contributions determined from the simultaneous fit of the physics channels to the selected $[pn]$ channel were subtracted. The resulting cross section was extrapolated over unmeasured regions, assuming that the angular distribution of $(pn)pp$ ab-

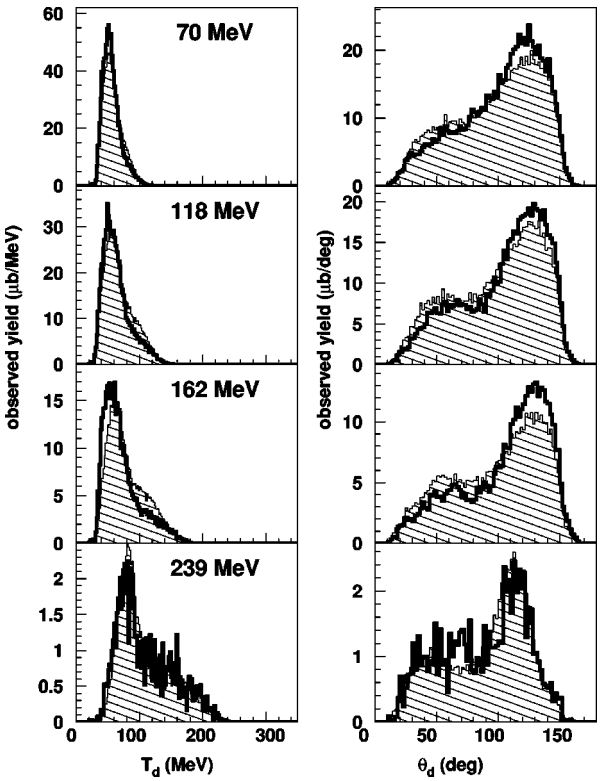

FIG. 7. The laboratory kinetic energy and θ distributions of the deuteron for the selected $[pd]$ channel, as in Fig. 2.

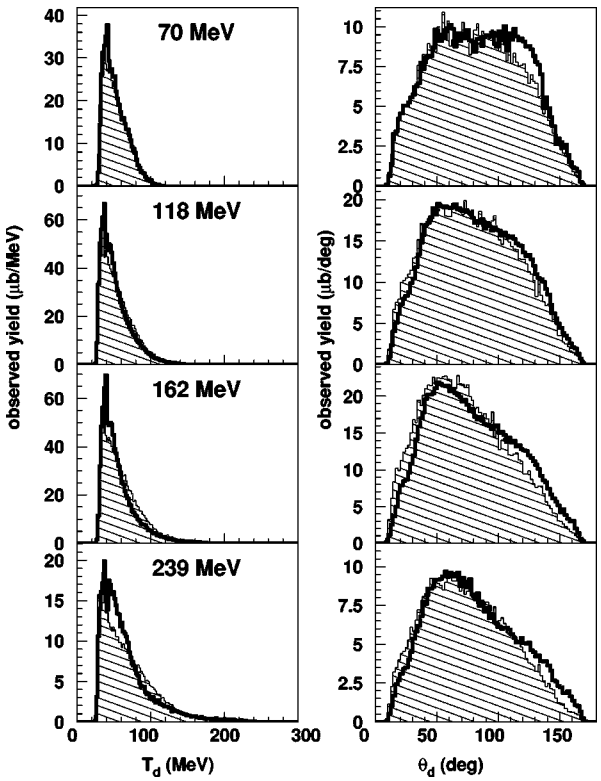

FIG. 9. The laboratory kinetic energy and θ distributions of the deuteron for the selected $[ppd]$ channel, as in Fig. 2.

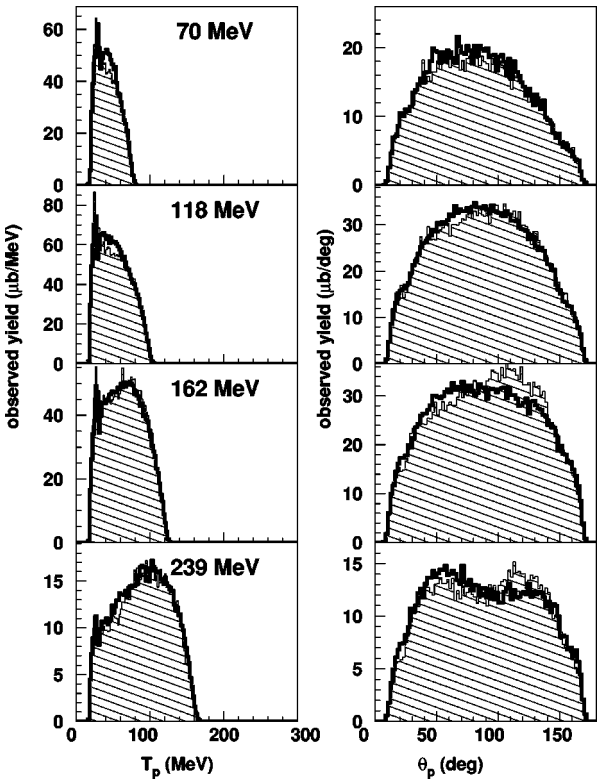

FIG. 10. The laboratory kinetic energy and θ distributions of the two protons for the selected $[ppd]$ channel, as in Fig. 2.

sorption is roughly the same as $(pp)pn$ absorption, and then multiplied by a factor of 3 to take into account in a rough manner the neutron detection efficiency. The uncertainty in the estimate of $(pn)pp$ was taken as half its value. The resulting cross section obtained in this analysis is consistent with the measured cross section of 1.85 ± 0.52 mb at 118 MeV of Ref. [19] for π^- absorption on ^{4}He leading to an energetic pn pair.

V. RESULTS

A. Total and partial absorption cross sections

The total pion absorption cross sections were determined from the global fit to the data (the quality of which is shown in Figs. 1–10). The results are shown in Fig. 11 along with the world data set, and the result of a Δ-hole model calculation [40] scaled by an arbitrary factor of 0.75. The present measurement at 118 MeV is in good agreement with that of Steinacher *et al.* [19], but is lower than the measurement of Baumgartner *et al.* [18]. The experiment of Ref. [18] measured the pion absorption cross section by subtraction of the cross section in which a charged pion was detected in the final state from the published total pion scattering cross sections [41]. Since neutral pions were not detected, this determination of the absorption cross section required an estimate of the single charge exchange cross section; this has recently been measured at 160 MeV [42] and found to be 5.5 mb larger than the estimate used in Ref. [18] at 170 MeV. However, even if the results of Ref. [18] are adjusted for this difference they remain higher than the total absorption cross sections presented here.

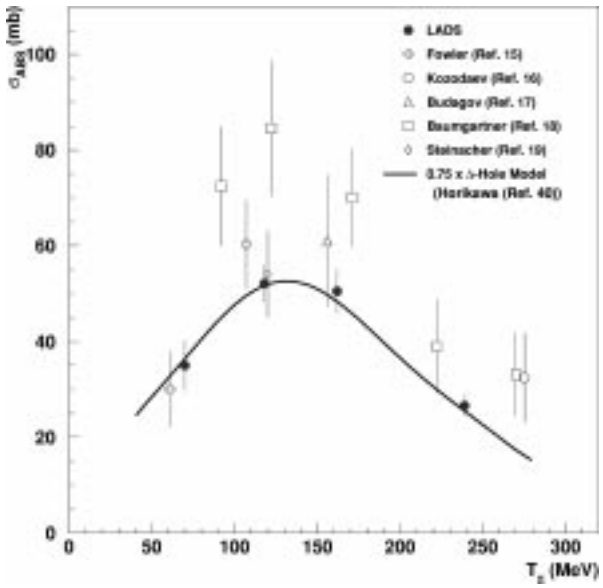

FIG. 11. The total absorption cross section on ^{4}He.

Based largely on Ref. [18] it had been previously suggested [43,44] that the total absorption cross section increased dramatically from ^{3}He to ^{4}He, possibly signaling the onset of a new absorption process available only in heavier nuclei. The results presented here exclude the possibility of such a dramatic rise.

The partial absorption cross sections for the various physics channels are presented in Table II. These cross sections were corrected for all detector inefficiencies, thresholds, and acceptance cuts. We have previously reported [39] precise values for the $pppn$ final state cross sections using more detailed models than those discussed here. These results are given in Table II for the four-body multinucleon channels $[(ppp)n$, $(ppn)p$, and $(pppn)]$. The agreement obtained for the cross section in the $pppn$ final state in the current global analysis, and that of Ref. [39] and in Table II, is within the quoted uncertainties (see Sec. V B). The uncertainties in the total and partial cross sections were obtained by combining in quadrature the fit procedure uncertainty and the normalization uncertainty, except for the $(pn)pp$ channel where a 50% uncertainty was assigned as described above.

B. Two-nucleon absorption

An overwhelming fraction of the cross section in the selected $[pp]$ channel comes from the 2NA process, which was simulated with the $(pp)d$ and $(pp)pn$ generators. The resolution of the missing mass in the experiment was not sufficient to separate events with a spectator deuteron from those with an unbound pn pair, as can be seen in Fig. 1.

The imposed requirement that the missing momentum be less than 250 MeV/c causes the missing mass of the unbound pn pair to peak near the pn endpoint, as can also be seen in the figure. Although it is apparent from the figure that the 2NA reaction preferentially leaves a deuteron spectator, it is also clear that the fraction with a pn pair spectator cannot be determined reliably with this method. It does, however, appear that the contribution from 2NA with an unbound spectator pn pair is relatively weak.

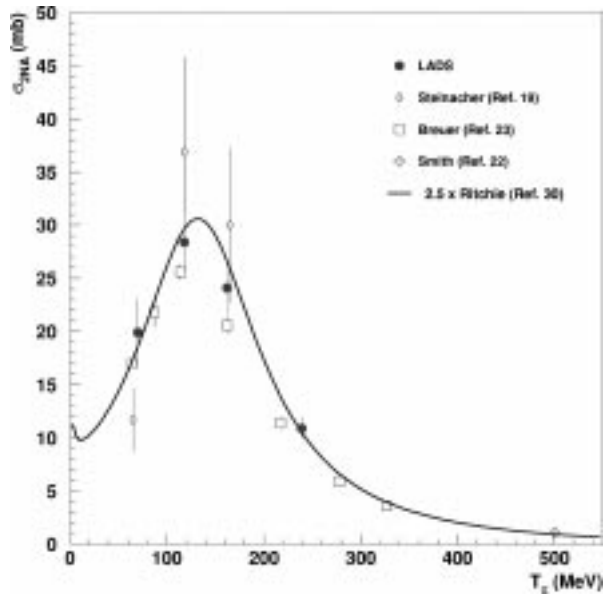

FIG. 12. The 2NA strength in pion absorption on ^{4}He.

Figure 2 shows that the result of the simultaneous fit to all channels gives a good description of the selected $[pp]$ data. Nevertheless, the separation between the $(pp)pn$ and other $pppn$ final states is not secure with the resolution of this experiment. The cross sections for the $pppn$ final states given in Table II are taken from Ref. [39] and differ slightly from those determined by the fits in this analysis. Hence the 2NA cross sections given here are those required for internal consistency between the total absorption cross section determined here and all other partial cross sections.

Figure 12 shows the absorption cross sections attributed to 2NA with either a d or pn pair spectator, along with the results from previous measurements [19,22,23]. The LADS measurement is in agreement with the existing data and the 2NA cross section is roughly 2.5 times the total absorption cross section on deuterium. The relative contribution of 2NA to the total absorption cross section falls as a function of energy from roughly 2/3 below the resonance to less than 1/2 well above the resonance. The falloff of the 2NA fraction of the total absorption cross section as a function of energy is consistent with absorption results obtained on heavier nuclei [45–51], which show a steady decrease as the incident energy rises. A similar behavior was observed in ^{3}He with the 2NA fraction falling from 86% at 70 MeV to 61% at 330 MeV [12].

C. Multinucleon absorption into four-body final states

The $pppn$ non-2NA absorption is comprised of three physics channels, two with one spectator nucleon, $(ppp)n$ and $(ppn)p$, and one in which all four nucleons participated, $(pppn)$. Figures 3–6 show the quality of the global fits in these channels. The sharp spikes at forward and backward angles in the neutron angular distributions come from the segmentation of the counters in the endcap region, and are reproduced by the simulation. The phase space representations of $(ppp)n$, $(ppn)p$, and $(pppn)$ appear to describe the data rather well, given their simplicity. There is a systematic tendency for the data to be more forward and backward peaked than the simulations. In Ref. [39] it is shown that agreement with the proton and neutron angular distributions can be improved by taking into account the orbital angular momentum of the incident pion [52]. Inclusion of ISI in the simulations of Ref. [39] also improved the agreement with the energy distributions, in particular for the $[ppp]$ channel at 239 MeV. However, for the integral quantities reported here, the discrepancies between the distributions obtained from the simple models and the data are not important.

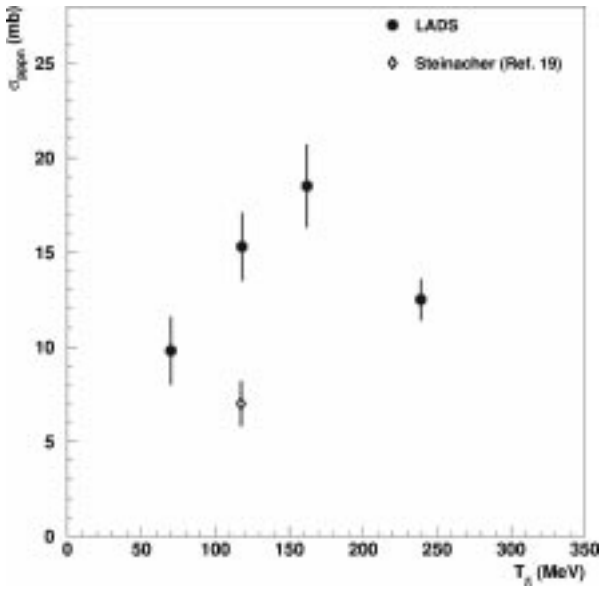

FIG. 13. The energy dependence of the cross section attributable to non-2NA processes leading to the four-body final state $pppn$.

The amount of cross section attributable to the $pppn$ final state is shown in Fig. 13. The cross section measured at 118 MeV by Steinacher *et al.* [19] is shown for comparison. The two channels in which three nucleons participate show resonancelike peaking (see Table II), and contribute the majority of the strength in the $pppn$ final state. The $(ppn)p$ process appears to dominate over the $(ppp)n$ process. As discussed

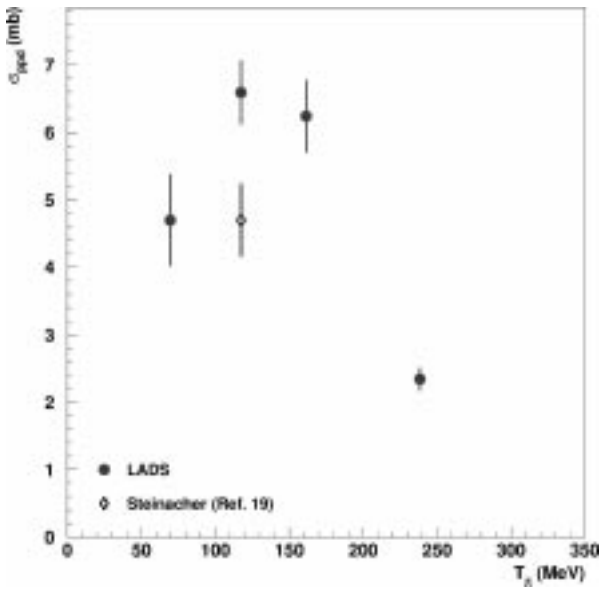

FIG. 14. The energy dependence of the cross section attributable to non-2NA processes leading to the three-body final state ppd.

in Ref. [39], the ratio of $(ppn)p$ to $(ppp)n$ is large at low energies (3.6 ± 1.2 at 70 MeV) and falls as the energy rises (1.4 ± 0.2 at 239 MeV). If final state interactions (FSI) comprised the bulk of the multinucleon cross section in this energy range then one could understand $(ppn)p$ being larger than $(ppp)n$ and also the fall of the ratio with energy. However, in this energy regime one expects πN interactions, and hence (ISI), to dominate over NN interactions (FSI). Initial state interactions (ISI) should by isospin arguments favor the $(ppp)n$ channel over the $(ppn)p$ channel, so that one may conclude that the mechanisms which lead to these cross sections are not yet understood. The contribution from the $(pppn)$ process, in which all four nucleons participate, appears to be small and nearly independent of incident pion energy, accounting for at most 18% of this yield at the highest energy. For a more detailed discussion of the $pppn$ non-2NA absorption channels see Ref. [39].

D. Multinucleon absorption with a deuteron in the final state

The non-2NA cross section in the ppd final state consists primarily of contributions from the $(pd)p$ and (ppd) channels. Figures 7 and 8 show the energy and angular distributions of deuterons and protons in the selected $[pd]$ channel, and those of the selected $[ppd]$ channel are shown in Figs. 9 and 10.

The distributions of the selected $[pd]$ channel appear to be consistent with absorption on a quasideuteron pair, followed by the pickup of a neutron by one of the outgoing protons. In such a picture the proton and deuteron are emitted roughly back-to-back with the deuteron preferentially at backward angles. The preference for the emission of the deuteron at backward angles can be qualitatively explained as being due to the smaller momentum transfer necessary for the pick-up reaction at these angles.

The selected $[ppd]$ channel (see Figs. 9 and 10) is somewhat more difficult to understand. The deuteron energy spectra are peaked toward lower energies than one would expect from simple phase space distributions, and the angular distributions of the deuterons become increasingly forward peaked with increasing pion energy. These observations suggest that the incoming pion initially scatters with a proton, which picks up a neutron to form a deuteron, while the pion is absorbed in the second step by the remaining pn pair. The magnitude of this channel, however, is difficult to understand as it is significantly larger than the reported cross section for ISI without pickup [10–12,39].

Another possible explanation for the deuteron's energy spectra being concentrated toward lower energies is that it is the result of an extended spectator momentum distribution, or that 2NA absorption tends to pick out portions of the wave function in which the spectator has a high initial momentum [53]. These arguments, however, are unable to explain the forward peaking of the deuteron angular distribution. More detailed comparisons with models are needed before a conclusion can be reached.

The cross section attributed to the ppd final state is shown in Fig. 14, again compared to the measurement of Ref. [19]. The energy dependence of the (ppd) cross section shows a broad resonancelike behavior, peaking somewhere between 118 and 162 MeV, and accounts for between 5 and 8 % of the total absorption cross section. The cross section attributable to the $(pd)p$ process is slightly smaller, and falls steadily with increasing incident pion energy.

VI. SUMMARY AND CONCLUSIONS

This paper has presented a measurement of the total absorption cross section for the absorption of positive pions on ^{4}He at 70, 118, 162, and 239 MeV. The total cross section was also decomposed into channels according to the number of participating nucleons and the final state. The largest contribution to the total cross section is attributed to 2NA, the contribution of which decreases as a function of energy from 2/3 of the total at 70 MeV to roughly 1/2 at 239 MeV.

The multinucleon absorption cross section was separated into two final states $pppn$ and ppd. The $pppn$ final state contribution to the total absorption cross section increases from about 25 to 50 % from the lowest to the highest measured energy, while the ppd final state contribution appears to fall slightly as a function of energy from 13% of the total absorption cross section at 70 MeV to 9% at 239 MeV.

While the measurement of the total absorption cross section on ^{4}He and its decomposition by number of spectators provide useful constraints on the magnitude of possible genuine multinucleon processes, the issue of whether the large non-2NA yield can be explained solely by sequential processes such as ISI and FSI remains unresolved. The ultimate answer to this question may be found only by a comparison of the measured total and partial absorption cross sections to realistic theoretical calculations.

ACKNOWLEDGMENTS

We thank the technical staff of the Paul Scherrer Institute for the support provided to this experiment. This work was supported in part by the German Bundesministerium für Forschung and Technologie (BMFT), the German Internationales Büro der Kernforschungsanlage Jülich, the Swiss National Science Foundation, the U.S. Department of Energy (DOE), and the U.S. National Science Foundation (NSF).

[1] H.J. Weyer, Phys. Rep. **195**, 295 (1990).
[2] Q. Ingram, Nucl. Phys. **A553**, 573c (1993).
[3] G. Backenstoss, M. Izycki, P. Salvisberg, M. Steinacher, P. Weber, H.J. Weyer, S. Cierjacks, S. Ljungfelt, H. Ullrich, M. Furić, and T. Petković, Phys. Rev. Lett. **55**, 2782 (1995).
[4] K.A. Aniol, A. Altman, R.R. Johnson, H.W. Roser, R. Tacik, U. Wienands, D. Ashery, J. Alster, M. A. Moinester, E. Piasetzky, D.R. Gill, and J. Vincent, Phys. Rev. C **33**, 1714 (1986).
[5] L.C. Smith, R.C. Minehart, D. Ashery, E. Piasetsky, M. Moinester, I. Navon, D.F. Geesaman, J.P. Schiffer, G. Stephens, B. Zeidman, S. Levinson, S. Mukhopadhyay, R.E. Segel, B. Anderson, R. Madey, J. Watson, and R.R. Whitney, Phys. Rev. C **40**, 1347 (1989).
[6] S. Mukhopadhyay, S. Levenson, R.E. Segel, G. Garino, D.

Geesaman, J.P. Schiffer, G. Stephans, B. Zeidman, E. Ungricht, H. Jackson, R. Kowalczyk, D. Ashery, E. Piasetsky, M. Moinester, I. Navon, L.C. Smith, R.C. Minehart, G.S. Das, R.R. Whitney, R. McKeown, B. Anderson, R. Madey, and J. Watson, Phys. Rev. C **43**, 957 (1991).

[7] P. Weber, G. Backenstoss, M. Izycki, R.J. Powers, P. Salvisberg, M. Steinacher, H.J. Weyer, S. Cierjacks, A. Hoffart, B. Rzehorz, H. Ullrich, D. Bosnar, M. Furić, T. Petković, and N. Šimičević, Nucl. Phys. **A534**, 541 (1991).

[8] H. Hahn, A. Altman, D. Ashery, G. Gefen, D.R. Gill, R.R. Johnson, R. Levy-Nathansohn, M.A. Moinester, M. Sevior, and R.P. Trelle, Phys. Rev. C **53**, 1074 (1996).

[9] T. Alteholz, D. Androić, G. Backenstoss, D. Bosnar, H. Breuer, A. Brković, H. Döbbeling, T. Dooling, W. Fong, M. Furić, P. A. M. Gram, N.K. Gregory, J.P. Haas, A. Hoffart, Q. Ingram, A. Klein, K. Koch, J. Köhler, B. Kotliński, M. Kroedel, G. Kyle, A. Lehmann, Z.N. Lin, G. Mahl, A.O. Mateos, K. Michaelian, S. Mukhopadhyay, T. Petković, R.P. Redwine, D. Rowntree, R. Schumacher, U. Sennhauser, N. Šimičević, F.D. Smit, G. van der Steenhoven, D.R. Tieger, R. Trezeciak, H. Ullrich, M. Wang, M.H. Wang, H.J. Weyer, M. Wildi, and K.E. Wilson, Phys. Rev. Lett. **73**, 1336 (1994).

[10] G. Backenstoss, D. Bosnar, H. Breuer, H. Döbbeling, T. Dooling, M. Purić, P.A.M. Gram, N.K. Gregory, A. Hoffart, Q. Ingram, A. Klein, K. Koch, J. Köhler, B. Kotliński, M. Kroedel, G. Kyle, A. Lehmann, A.O. Mateos, K. Michaelian, T. Petković, R.P. Redwine, D. Rowntree, U. Sennhauser, N. Šimičević, R. Trezeciak, H. Ullrich, M. Wang, M.H. Wang, H.J. Weyer, M. Wildi, and K.E. Wilson, Phys. Lett. B **379**, 60 (1996).

[11] D. Androić, G. Backenstoss, D. Bosnar, H. Breuer, H. Döbbeling, T. Dooling, M. Furić, P.A.M. Gram, N.K. Gregory, A. Hoffart, Q. Ingram, A. Klein, K. Koch, J. Köhler, B. Kotliński, M. Kroedel, G. Kyle, A. Lehmann, A.O. Mateos, K. Michaelian, T. Petković, R.P. Redwine, D. Rowntree, U. Sennhauser, N. Šimičević, R. Trezeciak, H. Ullrich, M. Wang, M.H. Wang, H.J. Weyer, M. Wildi, and K.E. Wilson, Phys. Rev. C **53**, R2591 (1996).

[12] A. Lehmann, D. Androić, G. Backenstoss, D. Bosnar, H. Breuer, H. Döbbeling, T. Dooling, M. Furić, P.A.M. Gram, N.K. Gregory, A. Hoffart, Q. Ingram, A. Klein, K. Koch, J. Köhler, B. Kotliński, M. Kroedel, G. Kyle, A.O. Mateos, K. Michaelian, T. Petković, M. Planinić, R.P. Redwine, D. Rowntree, U. Sennhauser, N. Šimičević, R. Trezeciak, H. Ullrich, M. Wang, M.H. Wang, H.J. Weyer, M. Wildi, and K.E. Wilson, Phys. Rev. C **55**, 2931 (1997).

[13] G. Brown, H. Toki, W. Weise, and A. Wirzba, Phys. Lett. **118B**, 39 (1982).

[14] B. Schwesinger, A. Wirzba, and G.E. Brown, Phys. Lett. **132B**, 269 (1983).

[15] E.C. Fowler, W.B. Fowler, R.P. Shutt, A.M. Thorndike, and W.L. Whittemore, Phys. Rev. **91**, 135 (1953).

[16] M.S. Kozodaev, M.M. Kulyukin, R.M. Sulyaev, A.I. Filippov, and Yu. A. Schcherbakov, Sov. Phys. JETP **11**, 200 (1960).

[17] Yu. A. Budagov, R.F. Ermolov, E.A. Kushnirenko, and V.I. Moskalev, Sov. Phys. JETP **15**, 824 (1962).

[18] M. Baumgartner, H.P. Gubler, G.R. Plattner, W.D. Ramsay, H.W. Roser, I. Sick, P. Zupranski, J.P. Egger, and M. Thies, Nucl. Phys. **A399**, 451 (1983).

[19] M. Steinacher, G. Backenstoss, M. Izycki, P. Salvisberg, P. Weber, H.J. Weyer, A. Hoffart, B. Rzehorz, H. Ullrich, M. Dzemidzić, M. Furić, and T. Petković, Nucl. Phys. **A517**, 413 (1990).

[20] P. Weber, J. McAlister, R. Olszewski, A. Feltham, M. Hanna, R. Johnson, M. Pavan, C. Ponting, F. Rozon, M. Sevior, V. Sossi, D. Vetterli, D. Humphrey, G. Lolos, Z. Papandreou, R. Tacik, D. Ottewell, G. Sheffer, G. Smith, Y. Mardor, and S. May-Tal, Phys. Rev. C **43**, 1553 (1991).

[21] F. Adimi, H. Breuer, B. Flanders, M. Khandaker, M. Khayat, P. Roos, D. Zhang, T. Bauer, J. Konijn, C. de Laat, G. Kyle, S. Mukhopadhyay, M. Wang, and R. Tacik, Phys. Rev. C **45**, 2589 (1992).

[22] L.C. Smith, R.C. Minehart, O.K. Baker, D.B. Day, K.L. Giovanetti, R. Lourie, R.M. Marshall, B. Milbrath, B.G. Ritchie, R.M. Sealock, D. Tedeschi, and S.T. Thornton, Phys. Rev. C **48**, R485 (1993).

[23] H. Breuer, M. Khayat, F. Adimi, B. Flanders, M. Khandaker, P. Roos, D. Zhang, T. Bauer, J. Konijn, C. de Laat, G. Kyle, S. Mukhopadhyay, M. Wang, and R. Tacik, Phys. Rev. C **49**, R2276 (1994).

[24] B. Rzehorz, G. Backenstoss, M. Džemidžic, M. Furić, A. Hoffart, T. Petković, H. Ullrich, H.J. Weyer, D. Weiser, and M. Wildi, Europhys. Lett. **34**, 103 (1996).

[25] T. Alteholz, D. Androić, G. Backenstoss, D. Bosnar, H. Breuer, A. Brković, H. Döbbeling, T. Dooling, W. Fong, M. Furić, P.A.M. Gram, N.K. Gregory, J.P. Haas, A. Hoffart, Q. Ingram, A. Klein, K. Koch, J. Köhler, B. Kotliński, M. Kroedel, G. Kyle, A. Lehmann, Z.N. Lin, G. Mahl, A.O. Mateos, K. Michaelian, S. Mukhopadhyay, T. Petković, M. Planinić, R.P. Redwine, D. Rowntree, R. Schumacher, U. Sennhauser, N. Šimičević, F.D. Smith, G. van der Steenhoven, D.R. Tieger, R. Trezeciak, H. Ullrich, M. Wang, M.H. Wang, H.J. Weyer, M. Wildi, and K.E. Wilson, Nucl. Instrum. Methods Phys. Res. A **373**, 374 (1996).

[26] A. Mateos, Ph.D. thesis, MIT, 1995.

[27] K. Wilson, Ph.D. thesis, MIT, 1995.

[28] R. Trezeciak, Ph.D. thesis, University of Karlsruhe, 1995.

[29] M. Kroedel, Ph.D. thesis, University of Basel, 1996.

[30] B.G. Ritchie, Phys. Rev. C **49**, 553 (1991).

[31] R. Schiavilla (private communication); R. Schiavilla, V.R. Pandharipande, and R.B. Wiringa, Nucl. Phys. **A449**, 219 (1986).

[32] J. Gillespie, *Final-State Interactions* (Holden-Day, San Francisco, 1965).

[33] B. Zeitnitz, R. Maschuw, and P. Suhr, Nucl. Phys. **A149**, 449 (1970).

[34] R. Taylor, *Scattering Theory* (Wiley, New York, 1972).

[35] K. Watson, Phys. Rev. **88**, 1163 (1952).

[36] A.B. Migdal, Sov. Phys. JETP **1**, 2 (1955).

[37] M.L. Goldberger and K.M. Watson, *Collision Theory* (Wiley, New York, 1964).

[38] E. M. Henley, *Conference Isobaric Spin in Nuclear Physics*, Tallahassee, 1966 (unpublished).

[39] A. Lehmann, D. Androić, G. Backenstoss, D. Bosnar, H. Breuer, H. Döbbeling, T. Dooling, M. Furić, P.A.M. Gram, N.K. Gregory, A. Hoffart, Q. Ingram, A. Klein, K. Koch, J. Köhler, B. Kotliński, M. Kroedel, G. Kyle, A.O. Mateos, K. Michaelian, T. Petković, M. Planinić, R.P. Redwine, D. Rowntree, U. Sennhauser, N. Šimičević, R. Trezeciak, H. Ullrich, M. Wang, M.H. Wang, H.J. Weyer, M. Wildi, and K.E. Wilson, Phys. Rev. C **56**, 1872 (1997).

[40] Y. Horikawa, M. Thies, and F. Lenz, Nucl. Phys. **A345**, 386 (1980).
[41] F. Binon, P. Duteil, M. Gouanere, L. Hugon, J. Jansen, J.P. Lagnaux, H. Palevsky, J.-P. Peigneux, M. Spighel, and J.-P. Stroot, Nucl. Phys. **A298**, 799 (1978).
[42] M. Wang, Ph.D. thesis, MIT, 1994.
[43] M. Thies, Proceedings of the Twenty-First LAMPF Users Meeting, Report No. LA-11248-C, 1987 (unpublished), p. 18.
[44] F. Lenz, Prog. Theor. Phys. Suppl. **91**, 27 (1987).
[45] R. Rieder, P.D. Barnes, B. Bassalleck, R.A. Eisenstein, G. Franklin, R. Grace, C. Maher, P. Pile, J. Szymanski, and W.R. Wharton, Phys. Rev. C **33**, 614 (1986).
[46] A. Altman, D. Ashery, E. Piasetzky, J. Lichtenstadt, A. Yavin, W. Bertl, L. Felawka, H. Walter, R. Powers, R. Winter, and J. Pluym, Phys. Rev. C **34**, 1757 (1986).
[47] W. Burger, E. Beise, S. Gilad, R. Redwine, P. Roos, N. Chant, H. Breuer, G. Ciangaru, J. Silk, G. Blanpied, B. Preedom, B. Ritchie, M. Belcher, K. Gotow, D. Lee, and H. Ziock, Phys. Rev. C **41**, 2215 (1990).
[48] R. Schumacher, P. Amaudruz, Q. Ingram, U. Sennhauser, H. Breuer, N. Chant, A. Feldman, B. Flanders, F. Khazaie, D. Mack, P. Roos, J. Silk, and G. Kyle, Phys. Rev. C **38**, 2205 (1988).
[49] S. Hyman, D. Mack, H. Breuer, N. Chant, F. Khazaie, B. Ritchie, P. Roos, J. Silk, P. Amaudruz, T. Bauer, Q. Ingram, G. Kyle, D. Renker, R. Schumacher, U. Sennhauser, and W. Burger, Phys. Rev. C **41**, R409 (1990).
[50] D. Mack, P. Roos, H. Breuer, H. Chant, S. Hyman, F. Khazaie, B. Ritchie, J. Silk, G. Kyle, P. Amaudruz, T. Bauer, Q. Ingram, D. Renker, R. Schumacher, U. Sennhauser, and W. Burger, Phys. Rev. C **45**, 1767 (1992).
[51] D. Rowntree, Ph.D. thesis, MIT, 1995.
[52] N. Šimičević and A. Mateos, Phys. Rev. C **51**, 797 (1995).
[53] T. Dooling, Ph.D. thesis, Old Dominion University, Norfolk, Virginia, 1995.